Experimental observation of super-Klein tunneling in phononic crystals

Yifan Zhu, Aurélien Merkel, Liyun Cao, Yi Zeng, Sheng Wan, Tong Guo, Zihao Su, Siyuan Gao, Haohan Zeng, Hui Zhang, et al.

Experimental observation of super-Klein tunneling in phononic crystals

Yifan Zhu[†1,2], Aurélien Merkel[†1], Liyun Cao[1], Yi Zeng[1], Sheng Wan[1], Tong Guo[1], Zihao Su[2], Siyuan Gao[2], Haohan Zeng[2], Hui Zhang*[2] and Badreddine Assouar*[1]

[1]*Université de Lorraine, CNRS, Institut Jean Lamour, F-54000 Nancy, France*

[2]*Jiangsu Key Laboratory for Design and Manufacture of Micro-Nano Biomedical Instruments, School of Mechanical Engineering, Southeast University, Nanjing 211189, China*

Abstract

We numerically and experimentally report the acoustic analogue of the super-Klein tunneling in a heterojunction of phononic crystals formed with Willis scatterers that exhibit pseudospin-1 Dirac cones. Compared to the pseudospin-1/2 Dirac cones, pseudospin-1 ones require in the band structure an additional flat band across the Dirac points. The conventional Klein tunneling, which is predicted in pseudospin-1/2 systems like graphene, consists of perfect transmission only under normal incidence through a potential barrier of any width. However, the super-Klein tunneling we evidence here, is defined for pseudospin-1 systems as a perfect transmission for all incidence angles at one single frequency within the energy barrier. This direct observation may have important implications in the exploration of the rich physics of pseudospin-1 quasiparticles.

These authors contributed equally: Yifan Zhu, Aurélien Merkel

Corresponding authors:
*seuzhanghui@seu.edu.cn
*badreddine.assouar@univ-lorraine.fr

The extraordinary electronic properties of graphene offer a fertile platform to explore the rich physics of the relativistic Dirac equation [1, 2]. Indeed, the C_{6v} symmetry of the two-dimensional honeycomb structure along with the time-reversal symmetry guarantees the existence of a Dirac degeneracy at the two points K and K' at the corners of the Brillouin zone which are characterized by the C_{3v} symmetry [3]. As a consequence, the fermionic charge carriers around these points behave as two-dimensional massless quasiparticles with pseudospin-1/2, which does not relate to the intrinsic spin of the electrons but refers to the spatial degrees of freedom of the wavefunction, and with conical bands that obey the Dirac equation. By breaking one of the symmetries, these quasiparticles become massive and topological phase transition with a plethora of accompanying phenomena can be

observed [2, 4]. Pseudospin-1/2 relativistic quasiparticles are known to feature extraordinary tunneling properties known as the Klein paradox where a barrier potential is perfectly transparent to Dirac particles under normal incidence [5–9]. Acoustic analogue of the Klein tunneling has been observed in a phononic heterojunction [10]. While the two states degeneracy is distinctive of pseudospin-1/2 quasiparticles, a three states degeneracy where two linear bands intersect with an additional flat band forms a Dirac point with a higher dimensionality and pseudospin value of one. Such Dirac cone forming pseudopin-1 systems are found in Dice [11], breathing [12] or Lieb lattices [13]. Pseudospin-1 systems have been experimentally obtained in optical Lieb lattices by placing bosonic cold atoms [14], photonic square lattices through accidental degeneracies [15, 16], photonic Lieb lattices [17–19], and with electronic Lieb lattices [20, 21]. The scattering properties of pseudospin-1 quasiparticles, different from those of pseudospin-1/2 quasiparticles, comprise a striking unity transmission through one potential barrier at its center frequency for all incident angles which is called the super-Klein tunneling (SKT) [11, 22–26]. However, despite experimental observation of pseudospin-1 system, direct observation of super-Klein tunneling still represents a serious endeavor.

In this letter, we take advantage of a two-dimensional (2D) triangular lattice (similar to the cases in Refs. [3, 27, 28]) with C_{3v}-symmetric Willis resonant scatterers to tackle the acoustic analogue of the super-Klein tunneling effect. The symmetry of the lattice alongside with the symmetry of the scatterers guarantee the existence of a Dirac cone at the corner of the Brillouin zone [3, 27, 28]. The key design mechanism is that, the internal resonance of the Willis scatterers adds one band in the band structure that can be tuned to be nearly flat, and to intersect with the two linear bands at the Dirac point. This provides us opportunities to achieve highly flat band with more flexibility compared to photonic crystals with conventional scatterers [29]. The intersection of the three bands forms the sought-after pseudospin-1 system. We then create a phononic heterojunction by sandwiching two different pseudospin-1 phononic crystals where the Dirac degeneracies take place at two different frequencies, thus creating a potential barrier. The transmission properties of acoustic wave through the phononic heterojunction is then investigated.

The 2D phononic heterojunction is constructed by a triangular arrangement of Willis scatterers as schematically shown in Fig. 1(a). Willis scatterers are subwavelength scatterers that couple monopole to dipole moments and for which the scattering requires cross coupling between acoustic pressure and velocity fields [30–32]. Here, the Willis scatterers are hollow cylinders with three necks, which are connected to the same internal cavity, with an angle of $2\pi/3$ between each, hence the C_{3v}-symmetry protecting the Dirac cones at the corner of the Brillouin zone. The internal cavity with the three necks induces a resonant mode that lead to the additional flat band, which can be tuned to intersect the two other linear bands at the corner of Brillouin zone, thus constructing the pseudospin-

1 system. Since the intersection with the flat band is not protected by symmetry but is dependent on parameters of the system, this degeneracy is considered as accidental. Varying the sizes of the scatterers allows one to shift the Dirac cones without changing the lattice constant a. By designing two pseudospin-1 systems using the two Phononic crystals PC1 and PC2 with Dirac frequencies f_1 and f_2, respectively, this gives the conditions to construct the phononic analogue of the potential barrier of height $V = f_2 - f_1$ and width D as shown in Fig. 1(b). The experimental implementation of the phononic heterojunction is shown in Fig. 1(c).

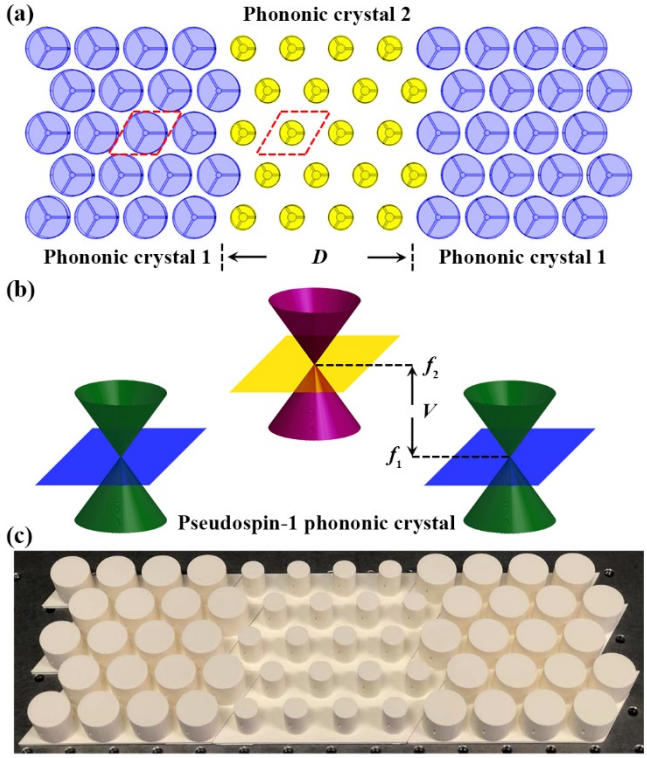

FIG. 1. Pseudospin-1 phononic crystals. (a) Scheme of the phononic heterojunction comprising two phononic crystals (PC1 and PC2) containing pseudospin-1 systems at different frequencies. The primitive cell is marked by red dashed lines. (b) Schematic diagram of the band spectrum corresponding the PC1 and PC2 with the potential barrier of width D and height $V = f_2 - f_1$. (c) Experimental structure of the phononic heterojunction.

In our system, the unit cells of the two phononic crystals PC1 and PC2 are composed of solid Willis scatterers, which can be considered as acoustically rigid, embedded in air as exposed in Fig. 2(a) and 2(b), respectively. The lattice constant is a = 2.8 cm. The height of the solid cylinders is limited to H = 2 cm, which ensures the two-dimensional character of the acoustic propagation in experiments. In more details, the scatterers in PC1 (PC2) are composed of cylinders with an external radius of R_1 = 1.2 cm (R_2 = 0.7 cm), with internal cavities of radius r_1 = 0.166 cm (r_2 = 0.256 cm). In both PC1 and PC2, the height of the internal cavities is h = 0.6 cm, and they are connected to the surrounding air by three rectangular necks of height h_0 = 0.4 cm and width w = 0.1 cm. The pseudospin-1 Dirac cones at the two different frequencies of the potential barrier are found by fine

tuning the external radiuses of the scatterers and the internal radiuses of the internal cavities. Indeed, the band structures of the two phononic crystals PC1 and PC2 exhibit Dirac cones at the K point at f_1 = 5.8 kHz and f_2 = 6.8 kHz as shown in Figs. 2(c) and (d), respectively. The linear bands are highlighted in red and the flat bands are highlighted in blue for PC1 and yellow for PC2. The height of the potential barrier is thus V = 1 kHz. To get more insight, we show in Fig. 2(e) the mode shape at the K point for PC2. The linear bands are associated with an acoustic pressure distribution that relates with the periodicity of the crystal, whereas the flat band is associated with the resonance of the scatterer for which the acoustic pressure is concentrated in the internal cavities of the scatterers.

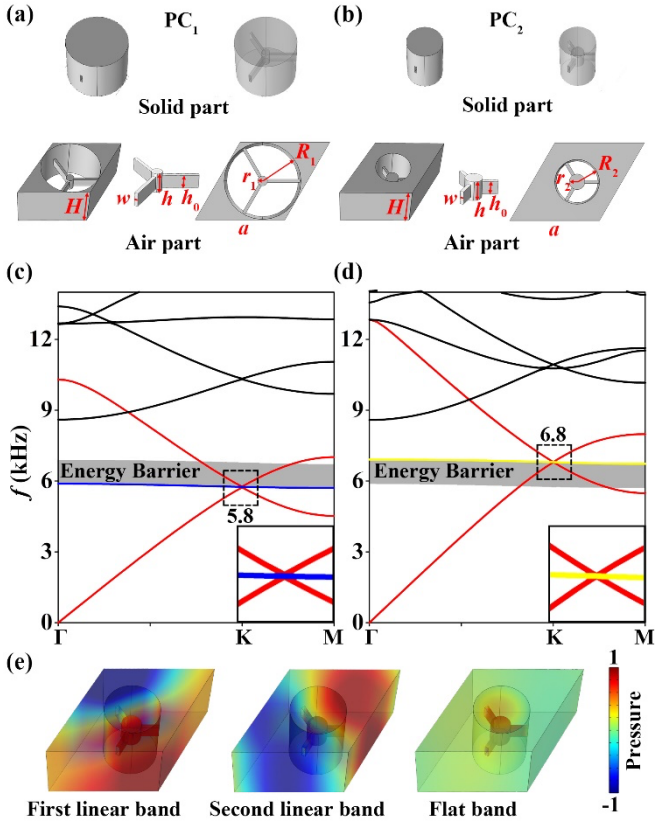

FIG. 2. (a-b) Unit cells of Phononic Crystal 1 (PC1) and Phononic Crystal 2 (PC2), respectively. (Solid and air parts are shown in the top and in the bottom, respectively.). While the height H, the internal dimensions w, h and h_0 are kept constant between PC1 and PC2, the band structure are modulated by the external radiuses R_1 and R_2 and internal radiuses r_1 and r_2 for PC1 and PC2, respectively. Band structures of (c) PC1 with a Dirac cone at f_1 = 5.8 kHz and (d) PC2 with a Dirac cone at f_2 = 6.8 kHz. The linear bands are highlighted in red, the flat bands are highlighted (c) in blue and (d) in yellow. The difference between the frequencies f_1 and f_2 gives the opportunity to create a heterojunction forming a potential barrier of height V = 1 kHz. (insets) Zoom around of the Dirac cones. (e) Acoustic pressure distributions in the unit cell of the three modes of PC2 at the K point and at the frequency f_2, corresponding to the two linear bands and the flat band.

The band structure around the K point is then described by the Hamiltonian [11, 22, 24-26]

$$H_1 = v_g \boldsymbol{S} \cdot \boldsymbol{k} \qquad (1)$$

where v_g is the group velocities, $\boldsymbol{k}$ is wavevector and the spin-one matrices are

$$\boldsymbol{S} = \boldsymbol{S_x x} + \boldsymbol{S_y y}, \text{ with } \boldsymbol{S_x} = \frac{1}{\sqrt{2}}\begin{pmatrix} 0 & 1 & 0 \\ 1 & 0 & 1 \\ 0 & 1 & 0 \end{pmatrix}, \text{and } \boldsymbol{S_y} = \frac{1}{\sqrt{2}}\begin{pmatrix} 0 & -i0 \\ -i0 & -i \\ 0 & -i0 \end{pmatrix} \quad (2)$$

the theoretical transmission of systems described by Eqs. (1) and (2) through a potential barrier at its center frequency, i.e., $f = f_1 + V/2$, is equal to unity for any incidence angle and any barrier width D. The potential barrier is introduced along one armchair direction of the crystal, which do not affect the transmission properties [10]. The numerical and experimental transmissions through a barrier width of 16.8 cm with an angle of incidence of 30° reveals a peak transmission at 6.4 kHz, whereas the transmission in the potential barrier, i.e., from 5.8 kHz to 6.8 kHz remains very low around $T = 0.2$ as shown in Fig. 3(a) (See supplemental materials, Notes 1 and 2). To further test the tunneling properties, the transmission at the frequency 6.4 kHz is numerically and experimentally measured as a function of the angle of incidence θ as shown in Fig. 3(b). The transmission is maximum for $\theta = 0^o$ and remains above $T = 0.81$ numerically, and $T = 0.84$ experimentally up to an angle of 30°. Above 30° incidence, the transmission decreases to reach the value $T = 0.5$ at an incidence angle of 60°. Transmission lower than unity for large incidence angles in contrast with the theoretical predictions has been observed in previous numerical simulations [11, 24]. For comparison, if the Willis scatterers are converted into cylindrical rigid scatterers, i.e. by removing the internal air cavities, the flat bands disappear from the band structures and Klein tunneling can be observed at normal incidence [10] (See supplemental materials, Note 3). As shown in Fig. S4, the transmission amplitude drops much faster with increasing incidence angle than in the case of SKT, thus supporting the efficiency of SKT. The transmission still exists at the boundary of the potential barrier at 5.8 kHz and 6.8 kHz as one can observe in Fig. 3(c), which is slightly different from the theoretical calculation for pseudospin-1 systems in electron systems provided in Ref. [11] (More details about the physical mechanism is discussed in supplemental materials, Note 4). In our system, the acoustic transmission is strongly reduced only in the frequency range within the potential barrier. Also, the frequency of maximum transmission in the potential barrier do not exactly correspond to its center frequency. Our pseudospin-1 systems differ from the theoretical modeling on several aspects. The flat bands are not perfectly flat. The group velocities v_g of the linear bands are not exactly equal between PC1 and PC2, and the Dirac cones of the real structures are slightly tilted. Tilted Dirac cones affect the tunneling properties in heterojunctions [33]. It is also worth mentioning the unavoidable effects of viscothermal losses. As a consequence, the theoretical model might not perfectly capture the wave propagation in the real fabricated structure. Nevertheless, the tunneling, while not completely angular independent, is still clearly visible for a broad range of incidence angles from 0^o up to 60^o, which differs drastically from the Klein tunneling where the transmission decreases much faster with increasing angle of incidence. We show in Fig. 3(c) the numerical acoustic pressure maps in the heterojunction corresponding the experimental setup shown in Fig. 3(d) for different frequencies with an incident

wave at an angle of 30°. In Fig. 3(e), one can see that the acoustic wave transmits through the barrier at 6.4 kHz, with an excellent agreement with the experimental measurements whereas it is mostly reflected at 6.1 kHz.

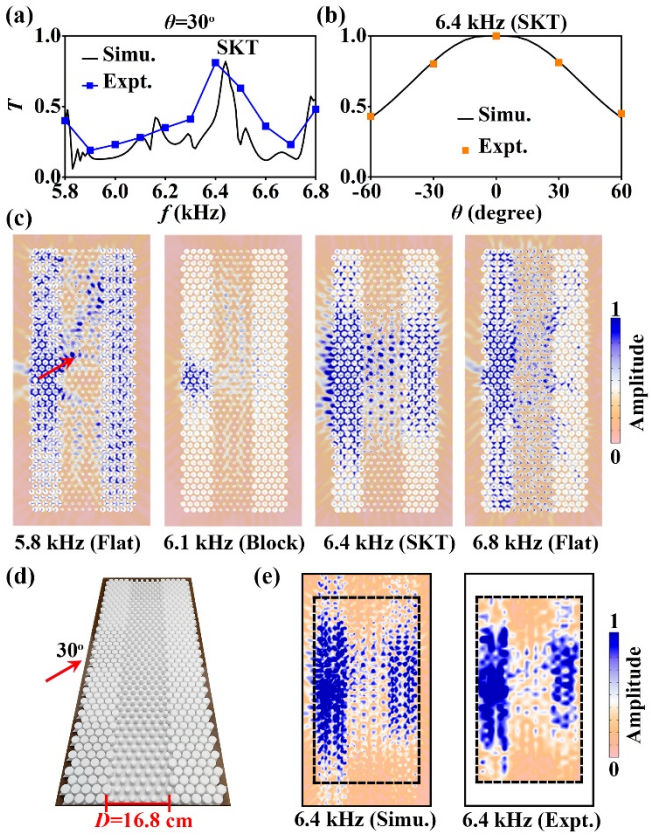

FIG. 3. Transmission through a potential barrier of width D = 16.8 cm. (a) Simulated (Simu.) and Experimental (Expt.) transmission T as a function of frequency with an angle of incidence $\theta = 30^{o}$ showing a peak at the frequency 6.4 kHz (b) Transmission at 6.4 kHz as a function of the angle of incidence. (c) Simulated acoustic pressure maps for 30° incidence at 5.8 kHz, 6.1 kHz, 6.4 kHz and 6.8 kHz, corresponding to lowest boundary of the potential barrier, a frequency which is blocked, Super-Klein Tunneling (SKT) frequency and the highest boundary of the potential barrier, respectively. (d) Photograph of the 3D printed sample. (e) Simulated (Simu.) and experimental (Expt.) acoustic field distributions for SKT at 6.4 kHz.

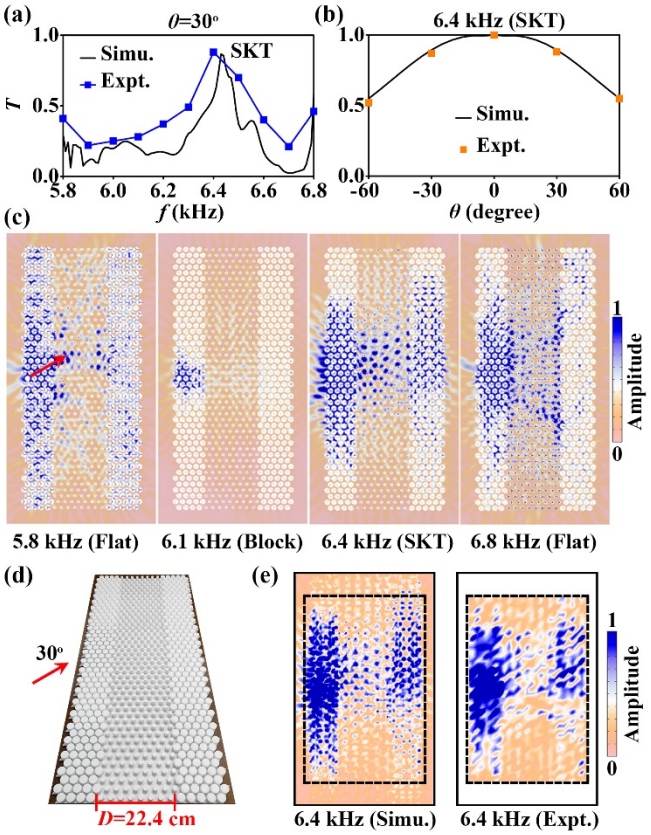

FIG. 4. Transmission through a potential barrier of width D = 22.4 cm. (a) Simulated (Simu.) and Experimental (Expt.) transmission T as a function of frequency with an angle of incidence $\theta = 30°$ showing a peak at the frequency 6.4 kHz (b) Transmission at 6.4 kHz as a function of the angle of incidence. (c) Simulated acoustic pressure maps for 30° incidence at 5.8 kHz, 6.1 kHz, 6.4 kHz and 6.8 kHz, corresponding to lowest boundary of the potential barrier, a frequency which is blocked, Super-Klein Tunneling (SKT) frequency and the highest boundary of the potential barrier, respectively. (d) Photograph of the 3-D printed sample. (e) Simulated (Simu.) and experimental (Expt.) acoustic field distributions for SKT at 6.4 kHz.

The super-Klein tunneling has the striking peculiarity to not depend on the barrier width. We now consider the case of wider barrier of a width of D = 22.4 cm. In Fig. 4(a), the transmission still presents a peak at 6.4 kHz with an angle of incidence of 30°. The transmission drops similarly when increasing the incidence angle like the case with a barrier width of D = 16.8 cm, as can be seen in Fig. 4(b). The acoustic pressure maps in Fig. 4(c) do not show drastic differences with this wider barrier compared to the one in Fig. 3(c). The experimental results using the structure shown in Figs. 4(d) are in excellent agreement with the numerical simulations as can be seen in Figs. 4(e). The dependence on the barrier width is further verified by simulating the transmission for an incidence angle of 30° with different barrier widths starting from 8.2 cm, which corresponds to 3 units wide, up to 22.4 cm, which corresponds to 8 units wide. The SKT is visible for each barrier width as shown in Fig. 5, which confirms that the transmission peak do not depend on the barrier width. Furthermore, this result

demonstrates that the mechanism of SKT is different from the conventional resonance transmission peak occuring when the barrier width corresponds to a multiple of half-wavelength.

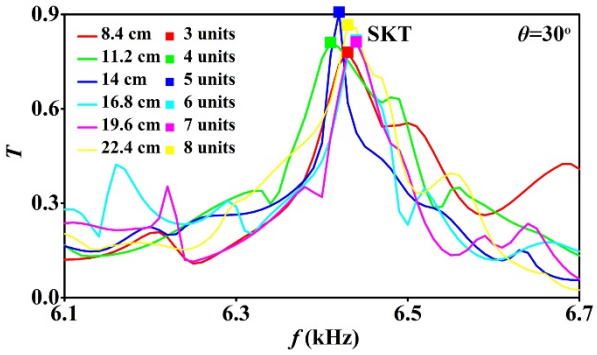

FIG. 5. Simulated transmissions with 30° incidence angle through potential barrier of different widths. The SKT effects can be observed with continuously variable widths from 8.4 cm to 22.4 cm, extending from 3 units to 8 units the PC2.

In summary, we have constructed and demonstrated the acoustic analogue of pseudospin-1 systems using phononic crystals composed of Willis scatterers. By changing the external and internal dimensions of the scatterers, the Dirac cones shift in frequency, which allowed us to build a heterojunction with a potential barrier. As key feature of pseudospin-1 quasiparticles, the transmission through the potential barrier exposes peak even at oblique incidences demonstrating the analogue of super-Klein tunneling in numerical simulations, which are in excellent agreement with the experimental measurements. Without the need of extreme low temperature or atom manipulation, phononic crystal with Willis scatterers represent a useful platform to investigate the rich physics of pseudospin-1 quasiparticles with, for instance, negative refraction effects with which it could be envisioned to build Veselago lenses [24, 26, 34, 35].

See supplemental material for details on the experimental measurements, numerical simulations, and discussions.

This work is supported by the Air Force Office of Scientific Research under award number FA9550-18-1-7021, and by la Région Grand Est and Institut Carnot ICEEL.

[1] K. S. Novoselov, A. K. Geim, S. V. Morozov, D. Jiang, M. I. Katsnelson, I. V. Grigorieva, S. V. Dubonos, and A. A. Firsov, Two-dimensional gas of massless dirac fermions in graphene, Nature **438**, 197 (2005).

[2] A. H. Castro, Neto, F.Guinea, N. M. R. Peres, K.S.Novoselov, andA.K.Geim, Theelectronic properties of graphene, Rev. Mod. Phys. **81**, 109 (2009).

[3] J. Lu, C. Qiu, S. Xu, Y. Ye, M. Ke, and Z. Liu, Dirac cones in two-dimensional artificial crystals for classical waves, Phys. Rev. B **89**, 134302 (2014).

[4] M. Z. Hasan and C. L. Kane, Colloquium: Topological insulators, Rev. Mod. Phys. **82**, 3045 (2010).

[5] O. Klein, Die reflexion von elektronen an einem potentialsprung nach der relativistischen dynamik von dirac, Z. Phys. **53**, 157 (1929).

[6] M. I. Katsnelson, K. S. Novoselov, and A. K. Geim, Chiral tunneling and the klein paradox in graphene, Nat. Phys. **2**, 620 (2006).

[7] A. F. Young and P. Kim, Quantum interference and klein tunneling in graphene heterojunctions, Nat. Phys. **5**, 222 (2009).

[8] N. Gao, J. Wang, and W. Q. Chen, Klein tunneling for Lamb waves in elastic phononic crystal plates. Appl. Phys. Lett., **121**, 102201 (2022).

[9] L. Sirota, Klein-like tunneling of sound via negative index metamaterials. Phys. Rev. Appl. **18**, 014057 (2022).

[10] X. Jiang, C. Shi, Z. Li, S. Wang, Y. Wang, S. Yand, S. G. Louie, and X. Zhang, Direct observation of klein tunneling in phononic crystals, Science **370**, 1447 (2020).

[11] D. F. Urban, D. Bercioux, M. Wimmer, and W. Haeusler, Barrier transmission of dirac-like pseudospin-one particles, Phys. Rev. B **84**, 115136 (2011).

[12] K. Essafi, L. D. C. Jaubert, and M. Udagawa, Flat bands and dirac cones in breathing lattices, J. Phys.: Condens. Matter **29**, 315802 (2017).

[13] M. Vigh, L. Oroszlany, S. Vajna, P. San-Jose, G. David, J. Cserti, and B. Dora, Diverging dc conductivity due to a flat band in a disordered system of pseudospin-1 dirac-weyl fermions, Phys. Rev. B **88**, 161413(R) (2013).

[14] S. Taie, H. Ozawa, T. Ichinose, T. Nishio, S. Nakajima, and Y. Takahashi, Coherent driving and freezing of bosonic matter wave in an optical lieb lattice, Sci. Adv. **1**, e1500854 (2016).

[15] X. Huang, Y. Lai, Z. H. Hang, H. Zheng, , and C. T. Chan, Dirac cones induced by accidental degeneracy in photonic crystals and zero-refractive-index materials, Nat. Mater. **10**, 582 (2011).

[16] P. Moitra, Y. Yang, Z. Anderson, I. I. Kravchenko, D. P. Briggs, and J. Valentine, Realization of an all-dielectric zero-index optical metamaterial, Nat. Phot. **7**, 791 (2013).

[17] D. Guzmán-Silva, C. Mejía-Cortés, M. A. Bandres, M. C. Rechtsman, S. Weimann, S. Nolte, M. Segev, A. Szameit, and R. A. Vicencio, Experimental observation of bulk and edge trans- port in photonic lieb lattices, New J. Phys. **16**, 063061 (2014).

[18] S. Mukherjee, A. Spracklen, D. Choudhury, N. Goldman, P. Ohberg, E. Andersson, and R.R. Thomson, Observation of a localized flat-band state in a photonic lieb lattice, Phys. Rev. Lett. **114**, 245504 (2015).

[19] R. A. Vicencio, C. Cantillano, L. Morales-Inostroza, B. Real, C. Mejia-Cortes, S. Weimann, A. Szameit, and M. I. Molina, Observation of localized states in lieb photonic lattices, Phys. Rev. Lett. **114**, 245503 (2015).

[20] R. Drost, T. Ojanen, A. Harju, and P. Liljeroth, Topological states in engineered atomic lattices, Nat. Phys. **13**, 668 (2017).

[21] M. R. Slot, T. S. Gardenier, P. H. Jacobse, G. C. P. van Miert, S. N. Kempkes, S. J. M. Zevenhuizen, C. M. Smith, D. Vanmaekelbergh, and I. Swart, Experimental realization and characterization of an electronic lieb lattice, Nat. Phys. **13**, 672 (2017).

[22] R. Shen, L. B. Shao, B. Wang, and D. Y. Xing, Single dirac cone with a flat band touching on line-centered-square optical lattices, Phys. Rev. B **81**, 041410(R) (2010).

[23] Y. Xu and G. Jin, Omnidirectional transmission and reflection of pseudospin-1 dirac fermions in a lieb superlattice, Phys. Lett. A **378**, 3554 (2014).

[24] A. Fang, Z. Q. Zhang, S. G. Louie, and C. T. Chan, Klein tunneling and supercollimation of pseudospin-1 electromagnetic waves, Phys. Rev. B **96**, 035422 (2016).

[25] Y. Betancur-Ocampo, G. Cordourier-Maruri, V. Gupta, and R. de Coss, Super-klein tunneling of massive pseudospin-one particles, Phys. Rev. B **96**, 024304 (2017).

[26] A. Fang, Z. Q. Zhang, S. G. Louie, and C. T. Chan, Pseudospin-1 physics of photonic crystals, Research **2019**, 3054062 (2019).

[27] J. Lu, C. Qiu, L. Ye, X. Fan, M. Ke, F. Zhang, and Z. Liu, Observation of topological valley transport of sound in sonic crystals, Nat. Phys. **13**, 369 (2017).

[28] Z. Wang, Y. Yang, H. Li, H. Jia, J. Luo, J. Huang, Z. Wang, B. Jiang, N. Yang, G. Jin, and H. Yang, Multichannel topological transport in an acoustic valley hall insulator, Phys. Rev. Applied **15**, 024019 (2021).

[29] C. T. Chan, Z. H. Hang, and X. Q. Huang, Dirac dispersion in two-dimensional photonic crystals, Adv. Optoelectron. **2012**, 313984 (2012).

[30] C. F. Sieck, A. Alu, and M. R. Haberman, Origins of willis coupling and acoustic bianisotropy in acoustic metamaterials through source-driven homogenization, Phys. Rev. B **96**, 104303 (2017).

[31] A. Merkel, V. Romero-Garcia, J.-P. Groby, J. Li, and J. Christensen, Unidirectional zero sonic reflection in passive pt-symmetric willis media, Phys. Rev. B **98**, 201102(R) (2018).

[32] A. Melnikov, Y. K. Chiang, L. Quan, S. Oberst, A. Alu, S. Marburg, and D. Powell, Acoustic meta-atom with experimentally verified maximum willis coupling, Nat. Commun. **10**, 3148 (2019).

[33] V. H. Nguyen and J. C. Charlier, Klein tunneling and electron optics in Dirac-Weyl fermion systems with tilted energy dispersion, Phys. Rev. B **97**, 235113 (2018).

[34] V. F. Vadim V. Cheianov and B. L. Altshuler, The focusing of electron flow and a veselago lens in graphene p-n junctions, Science **315**, 1252 (2007).

[35] G.-H. Lee, G.-H. Park, and H.-J. Lee, Observation of negative refraction of dirac fermions in graphene, Nat. Phys. **11**, 925 (2015).